


RESEARCH

Open Access



The histone deacetylase UvHOS2 regulates vegetative growth, conidiation, ustilaginoidin synthesis, and pathogenicity in *Ustilagoidea virens*

Zhaoyi Long¹, Peiyong Wang¹, Qianheng Yu¹, Bo Wang², Dayong Li¹, Cui Yang¹, Ling Liu¹, Guohua Duan^{1*} and Wenxian Sun^{1,2*} 

Abstract

Ustilagoidea virens causes rice false smut, one of the most devastating rice diseases. The pathogen produces various types of mycotoxins, such as ustilaginoidins and ustiloxins, which are harmful to both human and animal health. Histone deacetylases in fungi play an important role in regulating chromatin structure and gene expression. However, there is limited knowledge about how histone deacetylases control pathogenicity and mycotoxin biosynthesis in *U. virens*. Here, we characterize a putative class I histone deacetylase UvHOS2 in *U. virens*. The *UvHos2*-deletion mutants exhibit retarded vegetative growth, reduced conidial production and germination, and attenuated virulence. UvHOS2 positively regulates tolerance to various environmental stresses, including cell wall, cell membrane integrity, osmotic and oxidative stresses. UvHOS2 reduces the acetylation levels of histones at multiple Lys sites, including H3K9, H3K14, H3K27, and H3K56. ChIP-PCR assays revealed that UvHOS2-mediated H3K9 deacetylation regulates the expression of ustilaginoidin biosynthesis genes. Consistently, transcriptome analysis indicates that UvHOS2 regulates the expression of the genes involved in secondary metabolism, mycelial growth, conidiogenesis, and pathogenicity, thereby controlling *U. virens* virulence and mycotoxin (ustilaginoidins and sorbicillinoids) biosynthesis. This study provides a theoretical reference for revealing the epigenetic regulation of pathogenicity and mycotoxin biosynthesis in plant pathogenic fungi.

Keywords *Ustilagoidea virens*, Histone deacetylase, Pathogenicity, Ustilaginoidins, Biosynthesis

Background

Rice false smut caused by *Ustilagoidea virens* has recently become one of the most destructive fungal diseases in rice. The disease not only causes a severe yield loss but also threatens food safety due to the production of a variety of mycotoxins, such as ustiloxins and ustilaginoidins (Fu et al. 2017; Qiu et al. 2019). Ustilaginoidins consisting of at least 27 derivatives are a group of bis-naphtho- γ -pyrones, which are yellow or red powders easily soluble in organic solvents (Meng et al. 2015; Lai et al. 2019; Li et al. 2019b). The mycotoxins produced by *U. virens* have various biological activities, such as

*Correspondence:

Guohua Duan
ghduan1990@163.com
Wenxian Sun
wxs@cau.edu.cn

¹ College of Plant Protection, Jilin Provincial Key Laboratory of Green Management of Crop Pests and Diseases, Jilin Agricultural University, Changchun 130118, Jilin, China

² Department of Plant Pathology, Ministry of Agriculture Key Laboratory of Pest Monitoring and Green Management, College of Plant Protection, China Agricultural University, Beijing 100193, China



© The Author(s) 2024. **Open Access** This article is licensed under a Creative Commons Attribution 4.0 International License, which permits use, sharing, adaptation, distribution and reproduction in any medium or format, as long as you give appropriate credit to the original author(s) and the source, provide a link to the Creative Commons licence, and indicate if changes were made. The images or other third party material in this article are included in the article's Creative Commons licence, unless indicated otherwise in a credit line to the material. If material is not included in the article's Creative Commons licence and your intended use is not permitted by statutory regulation or exceeds the permitted use, you will need to obtain permission directly from the copyright holder. To view a copy of this licence, visit <http://creativecommons.org/licenses/by/4.0/>.

cytotoxicity, antibacterial, and immunosuppressive activities, and can cause embryonic malformations and mid-brain cell damage (Lu et al. 2015; Sun et al. 2017, 2020; Li et al. 2019b; Wang et al. 2021). The *ugs* gene cluster has been previously predicted and confirmed to be responsible for ustilaginoidin biosynthesis in *U. virens* (Zhang et al. 2014; Li et al. 2019b). However, little is known about the regulatory mechanisms of mycotoxin biosynthesis in *U. virens*, especially the regulatory roles of epigenetic modification in mycotoxin biosynthesis and pathogenicity. Therefore, an in-depth understanding of the regulatory mechanisms of ustilaginoidin biosynthesis in *U. virens* has an important scientific significance and a potential practical value for controlling this disease.

Histone acetylation/deacetylation is a common epigenetic modification that regulates multiple biological processes such as cell cycle, gene replication and transcription, secondary metabolism, and pathogenicity of pathogenic microorganisms. Histone acetyltransferases (HATs) and histone deacetylases (HDACs) cooperate to regulate histone acetylation and gene expression. Generally, HATs catalyze histone acetylation, which opens up chromatin to promote gene transcription, while HDACs mediate histone deacetylation, leading to a closed chromatin structure and "gene silencing" (Grunstein 1997). According to the classification rule of HDACs in yeast, fungal HDACs are mainly categorized into three classes: class I includes Reduced Potassium Dependency 3 (RPD3) and HOS2 (HDA One Similar 2); class II contains HDA1 (Histone Deacetylase 1) and HOS3; class III, also called Sirtuins, includes SIR2 (Silent Information Regulator 2) and HST1-4 (Homologue of SIR two) (Trojer et al. 2003; Ekwall 2005).

Recent studies have highlighted the involvement of histone deacetylases in regulating fungal pathogenicity and mycotoxin biosynthesis. For example, the HDAC gene *Rpd3* is silenced in *Magnaporthe oryzae*, causing delayed appressorium-mediated penetration, impaired invasive growth, and reduced pathogenicity (Lee et al. 2021). Similarly, knockdown of the *RpdA* gene results in attenuated pathogenicity in *Aspergillus fumigatus* (Bauer et al. 2019). In *Alternaria alternata*, the *Hos2* knockout mutant exhibits slow vegetative growth, retarded conidial development, and significantly reduced pathogenicity compared with the wild-type strain (Ma et al. 2021). In *Fusarium fujikuroi*, the knockout mutants of the class II deacetylase genes *Hda1* and *Hda2* are significantly attenuated in pathogenicity and show reduced biosynthesis of secondary metabolites, such as gibberellin and fusaric acid (Studt et al. 2013). Gene expression in the polyketide synthase (PKS) gene cluster involved in dihydroxynaphthalene-melanin biosynthesis is significantly decreased in the *Penicillium chrysogenum HdaA*-knockout mutant,

thus leading to a substantial reduction in conidial pigmentation (Guzman-Chavez et al. 2018). In contrast, some HDACs negatively regulate secondary metabolism. For instance, the targeted knockout of *HstD/Hst4* in *A. oryzae* results in a significant increase in penicillin and kojic acid production (Kawauchi et al. 2013). When the *Hda1* homologous genes are deleted, the production of 1,8-dihydroxy melanin, ergosterol, and deoxynivalenol is greatly promoted in *M. oryzae* and in *F. asiaticum*, respectively (Maeda et al. 2017). Therefore, various HDACs play different regulatory roles in pathogenicity and secondary metabolism.

Recently, progresses have been made on the molecular mechanisms of fungal HDACs in regulating pathogenicity and secondary metabolism. The deacetylase HosA in *A. flavus* interacts with the transcription factor SinA to form a complex that binds directly to the promoter in the aflatoxin B1 (AFB) biosynthetic gene cluster to positively regulate AFB biosynthesis (Lan et al. 2019). The GATA transcription factor Brg1 in *Candida albicans* recruits Hda1 to the promoters of hypha-specific genes to regulate hyphal development (Lu et al. 2012). In addition, elevated acetylation of H3K56 and H4K16 in *Beauveria bassiana* is essential for *Hos2*-regulated expression of genes for DNA damage repair, cell size, asexual development, and virulence (Cai et al. 2018). However, little is known how histone deacetylases, particularly for HOS2, function in regulating gene expression, secondary metabolism, and pathogenicity in phytopathogenic fungi. Therefore, it is important to investigate molecular mechanisms of epigenetic modification regulating ustilaginoidin biosynthesis and pathogenicity in *U. virens*.

In this study, we discover that *UvHos2* encoding a histone deacetylase is required for mycelial growth, conidia development, ustilaginoidin biosynthesis, and virulence. Besides, the levels of acetylation at H3K9, H3K14, H3K27, and H3K56 are elevated in the $\Delta Uvhos2$ mutant. Transcriptome and chromatin immunoprecipitation (ChIP)-qPCR analyses indicate that *UvHOS2* is involved in regulating the expression of the genes involved in secondary metabolism, mycelial growth, conidiogenesis, and pathogenicity, and thereby controls *U. virens* virulence and ustilaginoidin biosynthesis.

Results

UvHOS2 positively regulates mycelial growth and conidial production

The *U. virens* genome contains seven putative HDAC genes, among which *UVR_04561* is predicted to encode a histone deacetylase HOS2. To detect the evolutionary conservation of HOS2 homologs across fungal species, a phylogenetic tree was generated for type I histone deacetylases in *U. virens* and the related fungal species, such

as *B. bassiana*, *Ustilago maydis*, *F. graminearum*, *Saccharomyces cerevisiae*, *M. oryzae*, *A. alternata*, and *A. flavus* using the maximum likelihood method through MEGA X software (Additional file 1: Figure S1a). Based on the constructed tree, UvHOS2 is the most closely related to its orthologs in *B. bassiana* and *F. graminearum*. The HDAC structural domains were also predicted (Additional file 1: Figure S1b). To investigate the functions of *UvHos2*, the $\Delta Uvhos2$ knockout mutants were generated through the CRISPR/Cas9 system and homologous recombination (Additional file 1: Figure S2a). The *UvHos2*-knockout mutants were confirmed by Southern blot analyses (Additional file 1: Figure S2b). In addition, the complemented strains were generated by introducing the constructed plasmid carrying the *UvHos2* gene with the strong promoter of *UVR_08266* into the $\Delta Uvhos2$ mutant. Expression of UvHOS2-FLAG in these complemented strains was confirmed by western blot analysis (Additional file 1: Figure S2c).

Subsequently, we observed colony growth, hyphal morphology, conidial development, and germination in the wild-type, mutant, and complemented strains. Phenotypic analyses showed that the $\Delta Uvhos2$ strain exhibited a slower mycelial growth on potato sucrose agar (PSA) plates compared to the wild-type strain, while the growth of complemented strains was restored to the wild-type level (Fig. 1a). Furthermore, the interseptal distances in hyphae of the strains were measured after the hyphae were stained with the cell wall-specific dye Calcofluor White. We found that the $\Delta Uvhos2$ mutant had a shorter interseptal distance than the wild-type strain (Fig. 1b, c). The interseptal distance of the complemented strain was restored close to the wild-type level (Fig. 1b, c). To investigate the role of *UvHos2* in conidial production and germination in *U. virens*, we found that the $\Delta Uvhos2$ strain produced significantly fewer conidiospores than the wild-type strain, whereas the wild-type and complemented strains exhibited no difference in conidiogenesis (Fig. 1d). In addition, the conidia of the wild-type and complemented strains germinated at ~3 h, while the $\Delta Uvhos2$ conidia began to germinate at ~6 h. The germination rates of $\Delta Uvhos2$ were much lower than those of the wild-type and complemented strains at the tested time-points (Fig. 1e, f). Altogether, these results indicate that UvHOS2 plays an important role in hyphal growth and development, conidial development and germination.

***UvHos2* is essential for *U. virens* virulence and ustilaginoidin biosynthesis**

To investigate whether UvHOS2 is involved in virulence and pathogenicity, conidiospore suspensions prepared from the wild-type, $\Delta Uvhos2$, and complemented strains were injection inoculated into rice panicles of the variety

Changbai15 before heading. Disease symptoms were observed at four weeks after inoculation. The $\Delta Uvhos2$ mutant produced no false smut ball on the inoculated panicles. By contrast, the wild-type strain generated about ten false smut balls per inoculated panicle. The complemented strain partially restored the ability to produce false smut balls (Fig. 2a, b). These results indicate that the $\Delta Uvhos2$ mutant is significantly less pathogenic than the wild-type strain, suggesting a positive regulatory role of UvHOS2 in *U. virens* pathogenicity.

Furthermore, ustilaginoidins were extracted from four-week-old mycelial cultures of the wild-type, knockout mutant, and complemented strains and were then subject to HPLC analyses. The results showed that the $\Delta Uvhos2$ mutant produced a significantly lower amount of ustilaginoidins than the wild-type strain, and the complemented strain restored the ability to produce ustilaginoidins close to the wild-type level (Fig. 2c). The results indicate that UvHOS2 positively regulates the biosynthesis of ustilaginoidins.

***UvHos2* is involved in tolerance to various environmental stresses**

To investigate the role of *UvHos2* in response to various environmental stresses, the wild-type, $\Delta Uvhos2$, and complemented strains were cultured on yeast extract-tryptone (YT) medium plates containing different stressors, and mycelial growth was measured after 14 days of culturing. The $\Delta Uvhos2$ mutant exhibited a higher growth inhibition rate in the NaCl-containing medium than the wild-type strain, indicating that the $\Delta Uvhos2$ mutant is significantly more susceptible to salt osmotic stress. On the SDS-containing medium plates, the $\Delta Uvhos2$ strain was hypersensitive and exhibited almost no mycelial growth. In addition, the mutant was more susceptible to oxidative stress (0.07% H₂O₂) and Congo Red (70 µg/mL) than the wild-type and complemented strains, indicating an important role of UvHOS2 in tolerance to oxidative stress and in maintaining cell wall integrity (Fig. 3). Because HOS2 belongs to classical histone deacetylases, the sensitivity of the $\Delta Uvhos2$ mutant to the inhibitor trichostatin A (TSA) of classical HDACs was tested. We found that the growth inhibition rate of $\Delta Uvhos2$ was significantly greater than those of the wild-type and complemented strains. Altogether, these results indicate that *UvHos2* deletion causes *U. virens* to be more susceptible to the osmotic, cell membrane, cell wall and oxidative stressors, as well as the HDAC inhibitor.

UvHOS2 is involved in histone deacetylation

To investigate whether UvHOS2 is involved in histone deacetylation, we compared the acetylation levels at putative histone acetylation sites in the wild-type,

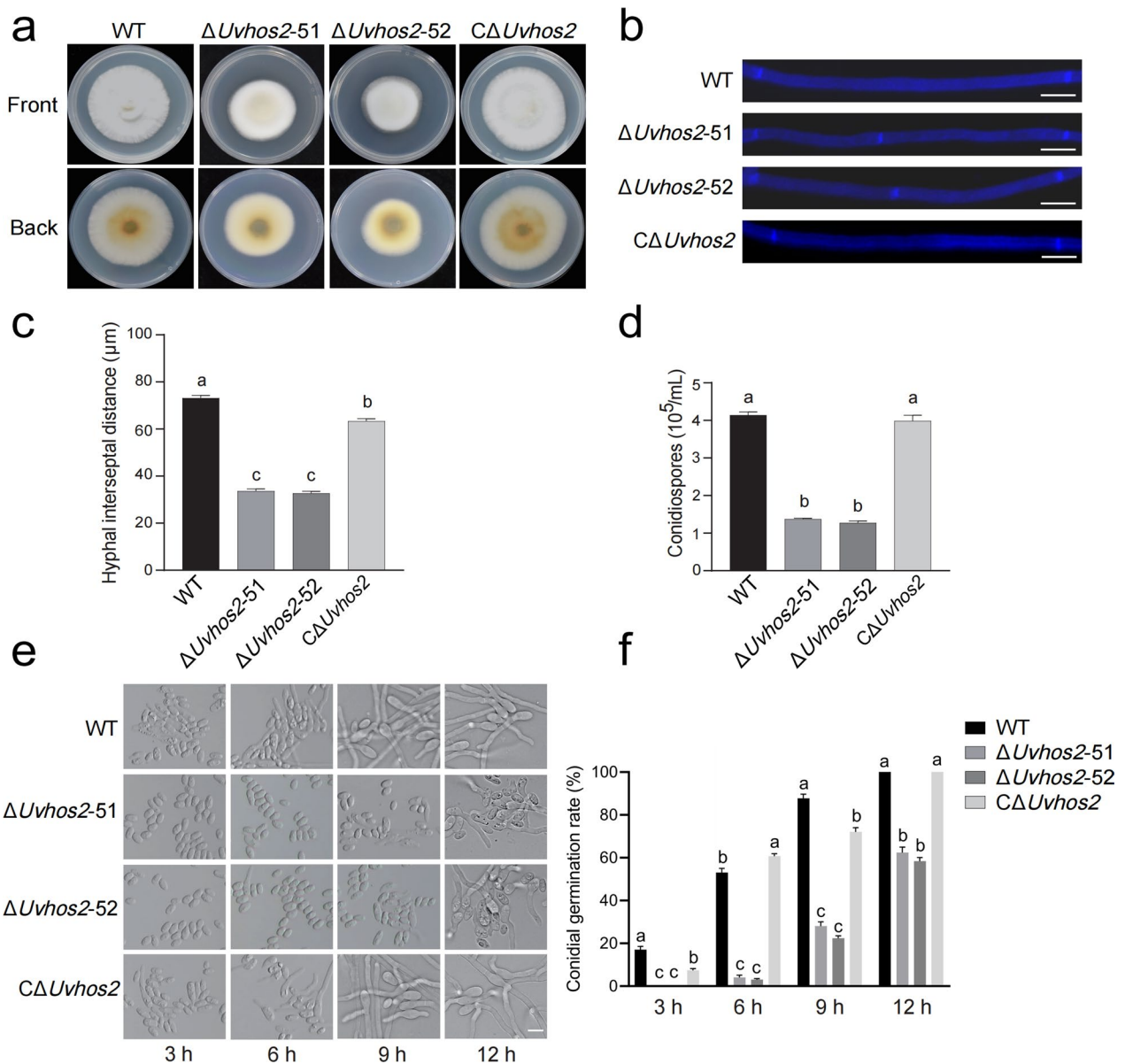


Fig. 1 UvHOS2 is required for hyphal growth, conidial development and germination in *U. virens*. **a** Colony morphology of the wild-type, $\Delta Uvhos2$ mutant, and $C\Delta Uvhos2$ complemented strains after culturing on PSA plates for 14 d. **b** The interseptal distance in the hyphae of the wild-type, $\Delta Uvhos2-51$, $\Delta Uvhos2-52$, and $C\Delta Uvhos2$ strains was observed by fluorescence microscopy. The hyphae were stained with Calcofluor White after conidia were germinated for 2 d. Scale bars: 20 μm . **c** The average interseptal distance of the wild-type, $\Delta Uvhos2-51$, $\Delta Uvhos2-52$, and $C\Delta Uvhos2$ strains. A total of 100 interseptum compartments were randomly selected and measured. Data are presented as mean \pm standard error (SEM) ($n = 100$). **d** The number of conidia generated by the wild-type, $\Delta Uvhos2-51$, $\Delta Uvhos2-52$, and $C\Delta Uvhos2$ strains after culturing in PSB medium for 7 d. Data are shown as mean \pm SEM ($n = 3$). **e** Spore germination was observed with microscopy for the wild-type, $\Delta Uvhos2-51$, $\Delta Uvhos2-52$, and $C\Delta Uvhos2$ strains from 3 to 12 h. Scale bars: 5 μm . **f** The conidial germination rates of the wild-type, $\Delta Uvhos2-51$, $\Delta Uvhos2-52$, and $C\Delta Uvhos2$ strains at the indicated time points. A total of 100 spores were randomly selected and observed. Data are shown as mean \pm SEM ($n = 3$). Different lowercase letters indicate statistically significant differences ($P < 0.05$, one-way ANOVA with Duncan's multiple comparisons)

mutant, and complemented strains through western blot analyses using site-specific anti-acetylation antibodies. The results showed that the acetylation levels at H3K9, H3K14, H3K27, and H3K56 in the $\Delta Uvhos2$ mutant were significantly higher than those in the wild-type and

complemented strains (Fig. 4a, b), whereas no evident alteration in the acetylation level at H3K18, H4K5, and H4K8 was detected in these strains. These data indicate that UvHOS2 might be involved in deacetylation of histone H3 at H3K9, H3K14, H3K27, and H3K56.

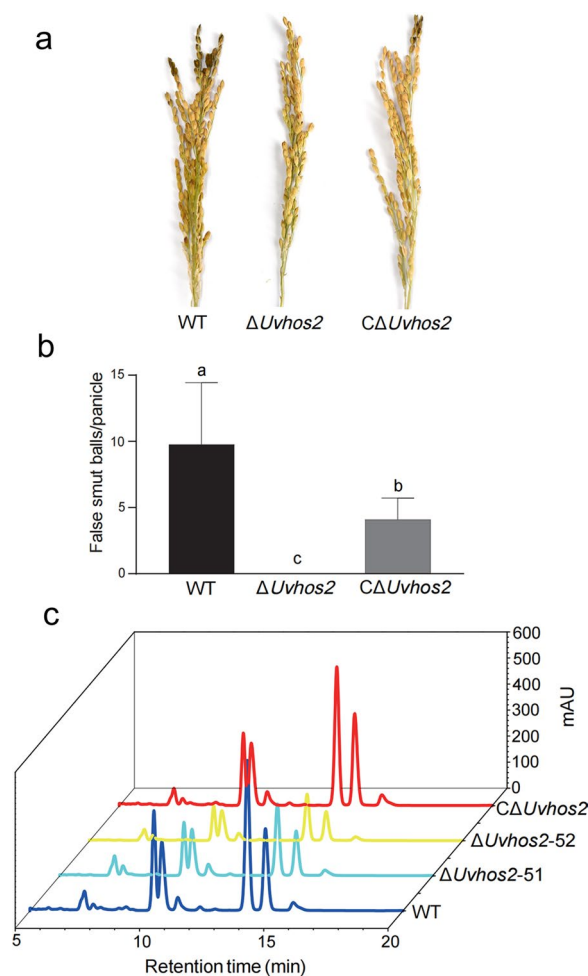


Fig. 2 UvHOS2 positively regulates pathogenicity and ustilaginoidin biosynthesis in *U. virens*. **a, b** The representative disease symptoms, and the average number of false smut balls per rice panicles after inoculation with the wild-type, $\Delta Uvhos2$, and the complemented strains. The images were captured, and the disease incidence rate and false smut balls were counted at four weeks after inoculation. The data from three independent assays are shown as mean \pm standard deviation (SD) ($n = 31, 30,$ and 33 for the wild-type, mutant, and complemented strains, respectively). Different lowercase letters indicate statistically significant differences ($P < 0.05$, one-way ANOVA with Duncan's multiple comparisons). **c.** HPLC assays to detect the amount of ustilaginoidins produced by the wild-type, $\Delta Uvhos2$ -51, $\Delta Uvhos2$ -52, and C $\Delta Uvhos2$ strains after 28 d of culturing on PSA plates

UvHOS2 regulates the expression of ustilaginoidin biosynthesis genes through H3K9 acetylation

To validate whether the elevated acetylation modification in the *Uvhos2* mutant is related to the expression of ustilaginoidin biosynthesis genes, chromatin immunoprecipitation (ChIP) was performed using an anti-acetyl-H3K9 antibody. ChIP-qPCR assays revealed that the enrichment of the promoters of ustilaginoidin biosynthesis

genes, including *UgsR1*, *UgsR2*, *UvPKS1*, *UgsL*, *UgsZ*, *UgsT*, and *UgsJ*, were significantly reduced in the *Uvhos2* mutant compared with the wild-type strain (Fig. 5a). In addition, the promoters of some up-regulated genes including *UV8b_01772*, *UV8b_03320*, and *UV8b_01755* were enriched by anti-acetyl-H3K9 antibody in the mutant strain compared with the wild type (Fig. 5b). The results demonstrated that UvHOS2 regulates the expression of ustilaginoidin biosynthesis genes by affecting H3K9 acetylation in *U. virens*.

UvHOS2 regulates the expression of the genes involved in mycotoxin biosynthesis

To investigate whether UvHOS2 plays a regulatory role in secondary metabolism, transcriptome analyses of the wild-type and $\Delta Uvhos2$ mutant strains were performed. Based on Fragments Per Kilobase of exon model per Million mapped fragments (FPKM) values, 2090 differentially expressed genes (DEGs), including 698 down-regulated and 1392 up-regulated genes, were identified according to the criteria of $P < 0.05$ and $|\text{Fold Change}| > 1.5$. A volcano plot showed differences in gene expression levels between the wild-type and $\Delta Uvhos2$ strains (Additional file 1: Figure S3).

The DEGs that might be involved in mycotoxin biosynthesis were clustered and analyzed (Fig. 6). The heatmaps illustrated the expression profiles of the genes involved in the biosynthesis of multiple secondary metabolites, such as ustilaginoidins (Fig. 6a) and sorbicillinoids (Fig. 6b). Besides, various types of cytochrome P450 genes (Fig. 6c) and non-ribosomal peptide synthetase genes (Fig. 6d) involved in secondary metabolism were also differentially expressed. Remarkably, the majority of these genes were transcriptionally suppressed in the $\Delta Uvhos2$ mutant.

Furthermore, RT-qPCR assays confirmed that six cytochrome P450 genes (*UV8b_06946*, *UV8b_05248*, *UV8b_00584*, *UV8b_00265*, *UV8b_04719*, and *UV8b_00540*), three polyketide synthase genes (*UV8b_07639*, *UV8b_01587*, and *UV8b_01594*), and two non-ribosomal peptide synthase genes (*UV8b_03234* and *UV8b_07622*) were down-regulated in the mutant strain (Fig. 6e). The results suggest that UvHOS2 plays an important role in secondary metabolism.

Transcriptome analyses also revealed that the redox-related genes *UgsL* and *UgsZ* in the *ugs* gene cluster were down-regulated when *Uvhos2* was deleted. RT-qPCR assays also revealed that the expression of the tested genes in the *ugs* gene cluster was significantly down-regulated in the $\Delta Uvhos2$ mutant compared with the wild-type strain. In contrast, the expression of these genes in the complemented strain was completely or partially restored to the wild-type level (Fig. 6f). Taken together, the results indicate that UvHOS2 positively regulates

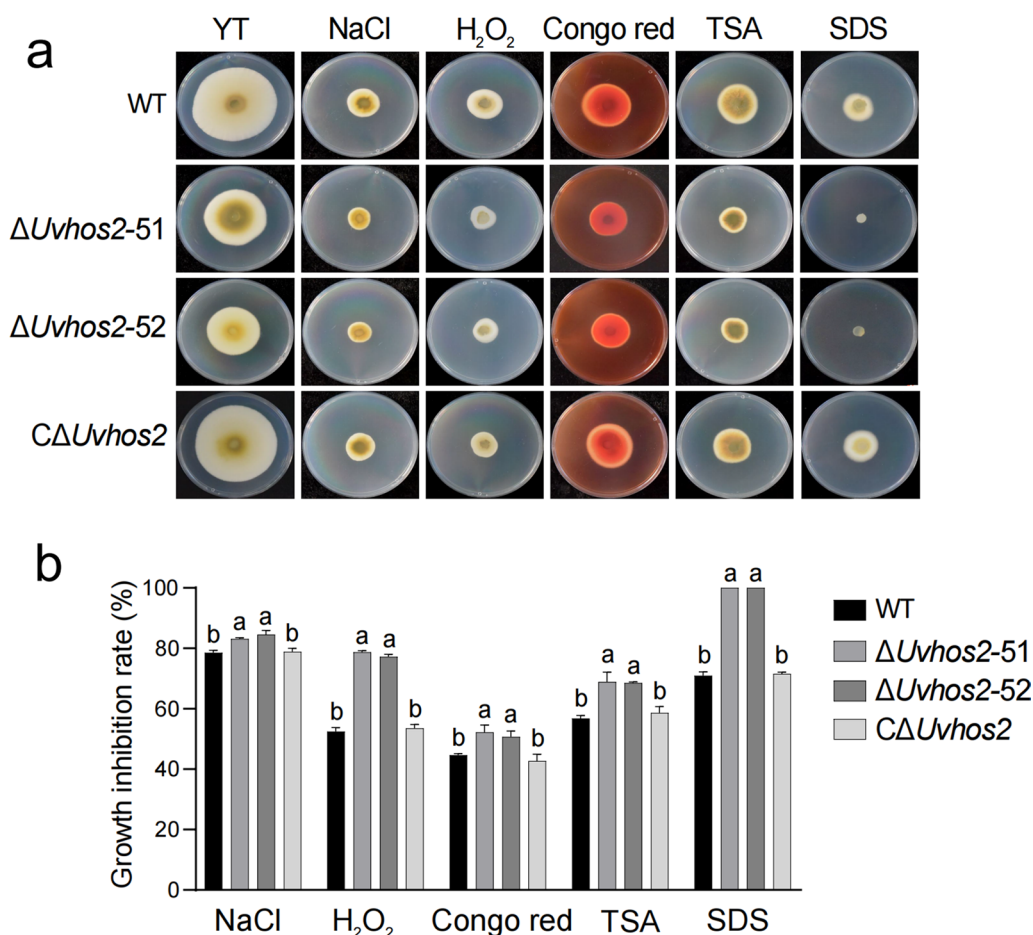


Fig. 3 UvHOS2 positively regulates tolerance to cell membrane, cell wall, hyperosmotic, and oxidative stresses in *U. vires*. **a** Colony morphologies of the wild-type, $\Delta Uvhos2-51$, $\Delta Uvhos2-52$, and complemented strains after culturing on YT medium plates containing various environmental stress factors (0.5 M NaCl, 0.03% SDS, 0.07% H₂O₂, 70 μ g/mL Congo Red, or 1 μ M TSA) for 14 d. **b** The growth inhibition rates of the wild-type, $\Delta Uvhos2-51$, $\Delta Uvhos2-52$, and complemented strains on YT medium plates containing different environmental stress factors. The representative data from three biological replicates are shown as mean \pm SEM (n = 3). Different letters indicate significant differences in the growth inhibition rates according to Duncan's test

ustilaginoidin biosynthesis through regulating gene expression in the *ugs* gene cluster.

Transcriptome analysis reveals the Gene Ontology (GO) terms and Kyoto Encyclopedia of Genes and Genomes (KEGG) pathways that might be regulated by UvHOS2

To uncover the regulatory mechanism of UvHOS2 on pathogenicity, mycotoxin biosynthesis, and tolerance to environmental stimuli, the GO terms and KEGG pathways enriched in down-regulated and up-regulated genes were identified through GO and KEGG pathway enrichment analyses. The down-regulated genes were enriched in such biological processes as cellular response to chemical stimulus, monocarboxylic acid metabolic process, organic hydroxy compound metabolic/biosynthetic process, fatty acid biosynthetic/metabolic process, and

MAPK cascade. At the molecular functional level, these genes were predominantly associated with DNA binding, such as sequence-specific DNA binding, RNA polymerase II transcription regulatory region sequence-specific DNA binding, transcription regulatory region nucleic acid binding, transcription *cis*-regulatory region binding, and DNA-binding transcription factor activity (Fig. 7a). As revealed by KEGG enrichment analysis, the down-regulated genes were primarily involved in such pathways as transporters, protein kinases, MAPK signaling pathway, and transcription factors (Fig. 7b). By contrast, the upregulated genes are primarily associated with such biological processes related to rRNA processing and maturation, and ribosome biogenesis. At the cellular component level, the upregulated genes were involved in biosynthesis of ribosomes and preribosomes, nuclear pore and ribonucleoprotein complex, while these genes were

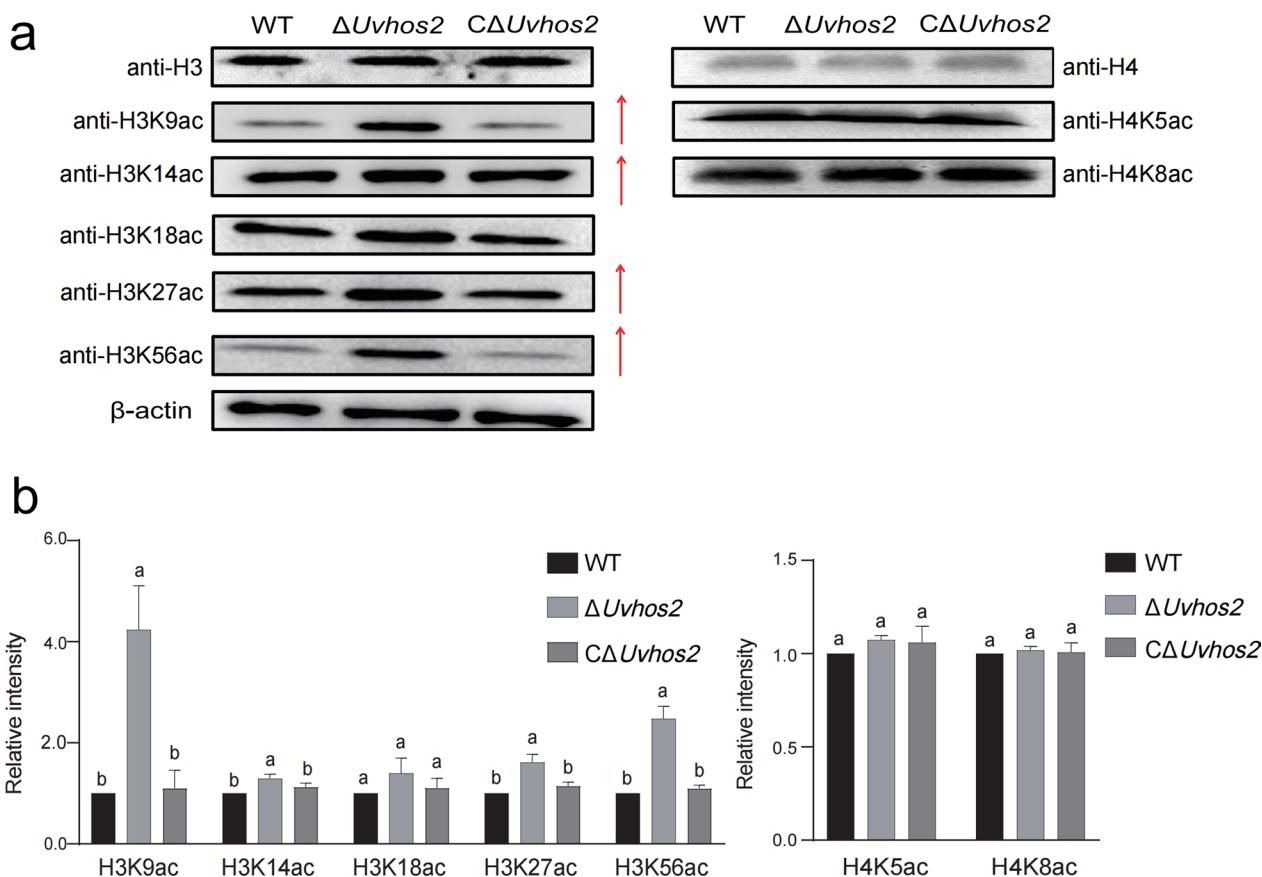


Fig. 4 UvHOS2 is involved in histone deacetylation at H3K9, H3K14, H3K27, and H3K56 in *U. vires*. **a** Western blot analyses to detect the acetylation levels at different Lys residues of H3 and H4 in the wild-type, mutant, and complemented strains using the indicated site-specific anti-acetylation antibodies. β-actin, H3, and H4 proteins were also detected as internal controls through western blotting. **b** The relative acetylation levels at different Lys residues in H3 and H4 were quantified by densitometry using ImageJ. Data from three biological replicates are shown as mean ± SEM (n = 3). Different lowercase letters indicate statistically significant differences in the site-specific acetylation levels among different strains ($P < 0.05$, one-way ANOVA with Duncan's multiple comparisons)

associated with such molecular functions as RNA binding and RNA polymerase activity (Fig. 7c). The abnormal activity of ribosome and RNA metabolism may disrupt cellular and biological processes and alter normal metabolic regulatory networks in fungi. Consistently, KEGG analysis found that the upregulated genes were primarily associated with ribosome biogenesis, mRNA biogenesis, cysteine and methionine metabolism, and valine, leucine and isoleucine biosynthesis, and RNA polymerase (Fig. 7d). Collectively, transcriptome analyses identify multiple molecular functions and signaling pathways that may be affected by *UvHos2* mutation and provide insights into the regulatory mechanisms of UvHOS2 on pathogenicity, stimulus responses, and mycotoxin biosynthesis.

Weighted gene co-expression network analysis reveals key factors involving in ustilaginoidin biosynthesis

To further identify the co-expression gene modules regulated by UvHOS2, we performed a weighted gene

co-expression network analysis (WGCNA) based on the transcriptomic data (Fig. 8). Interestingly, a characteristic MEblue module ($r = -0.99$, $P < 0.01$) was found to contain multiple genes in the ustilaginoidin biosynthesis gene cluster, including *UgsR1*, *UgsJ*, *UgsH*, *UgsL*, *UgsT*, and *UvPKS1* (Fig. 8a). These ustilaginoidin biosynthesis-related genes were associated with 34 up-regulated and 176 down-regulated genes in the co-expression module, including 7 putative transcription factor-encoding genes *UV8b_04276*, *UV8b_03854*, *UV8b_02623*, *UV8b_03158*, *UV8b_00617*, *UV8b_00546*, and *UV8b_00825* (Fig. 8b). The annotation of these DEGs provided insights into their functions (Additional file 2: Table S1). The up-regulated genes were involved in the synthesis of ergosterol (*UV8b_07747*, ergosterol biosynthesis ERG4/ERG24 family), hydrolysis of carbohydrates (*UV8b_04720*, glycosyl hydrolase family 32), the phenol hydroxylase (*UV8b_05045*, phenol hydroxylase,

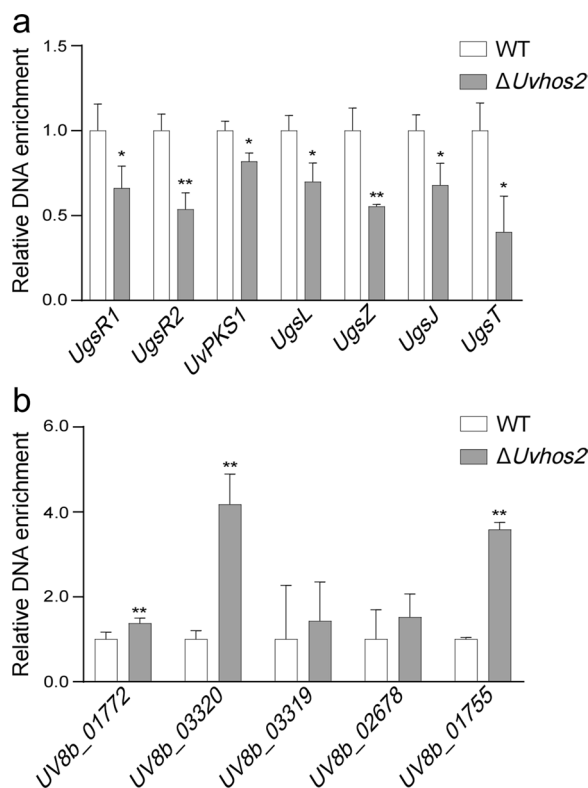


Fig. 5 ChIP-qPCR assays to show relative enrichment of ustilaginoidin biosynthesis genes and some up-regulated genes by acetylated H3K9 in the wild-type and $\Delta Uvhos2$ mutant strains. **a, b** The relative enrichment of the promoters of ustilaginoidin biosynthesis genes and some up-regulated genes by acetylated H3K9 in the wild-type and $\Delta Uvhos2$ mutant strains. Chromatin fragments were immunoprecipitated with an anti-H3K9ac antibody. Quantitative PCR was performed with the primers specific for the promoters of different genes listed in Additional file 2: Table S3. Representative data from three biological replicates are shown as mean \pm SD ($n=3$). *, $P < 0.05$ and **, $P < 0.01$ indicate significant and highly significant differences between the wild-type and mutant strains (Student's t -test)

C-terminal dimerisation domain), signaling processes (*UV8b_02672*, pleckstrin homology domain) or transcription regulation (*UV8b_04276*, transcription factors). The down-regulated genes were predicted to associate with a wide array of functions, such as metabolism of various compounds (*UV8b_00584*, cytochrome P450), biosynthesis of polyketides (*UV8b_01134*, acyl transferase domain in polyketide synthase enzymes; *UV8b_03322*, polyketide synthase), biosynthesis of aromatic amino acids (*UV8b_07897*, prephenate dehydrogenase), epigenetic regulation of gene expression (*UV8b_00355*, methyltransferase domain) and transcription regulation (*UV8b_02623*, *UV8b_03854*, *UV8b_00546*, *UV8b_00617*, *UV8b_00825*, *UV8b_03158*, transcription factors). Collectively, we

identified key factors associated with ustilaginoidin biosynthesis, and functional annotation has revealed their potential roles in this process, notably including transcription factors involved in gene expression regulation. These findings provide important clues for understanding the regulatory mechanisms of UvHOS2 in ustilaginoidin biosynthesis.

Discussion

Histone deacetylases in phytopathogenic fungi play important roles in hyphal growth and development, secondary metabolism, and virulence through distinct mechanisms (Baidyaroy et al. 2001; Tribus et al. 2010; Hnisz et al. 2012). In this study, we show that the HDAC UvHOS2 globally regulates vegetative growth, conidial development and germination, response to environmental stresses, secondary metabolism, and pathogenicity in *U. virens*. Transcriptome and ChIP-qPCR analyses reveal that UvHOS2 regulates the expression of the genes involved in ustilaginoidin biosynthesis and pathogenicity partially through affecting H3K9 acetylation.

The class I HDACs HOS2 and RPD3 in *U. virens* have the closest homologs in *B. bassiana* among the closely related fungi (Additional file 1: Figure S1). In consistent with the reduced ability to produce conidia and attenuated virulence in the $\Delta Uvhos2$ strain, the $\Delta hos2$ mutant in *B. bassiana* shows altered conidial properties, reduced conidiation capacity and virulence (Cai et al. 2018). Interestingly, *BcRpd3* overexpression in *Botrytis cinerea* also causes defects in growth, conidial germination and pathogenicity (Zhang et al. 2020). Interestingly, *MoRpd3* overexpression in *M. oryzae* leads to increased conidiation but loss of pathogenicity (Lin et al. 2021). Therefore, fungal class I HDACs play a significant role in asexual reproduction and pathogenicity.

The shorter hyphal interseptal spacing and slower mycelial growth in the $\Delta Uvhos2$ mutant indicate that *UvHos2* plays a crucial role in vegetative growth. Consistently, *Hos2* and *Rpd3* in *A. alternata* are required for fungal growth and conidiation (Ma et al. 2021). In *M. oryzae*, the deletion of *MoHst4* results in a significant reduction in mycelial growth and conidial development (Lin et al. 2021). In contrast, *Hos2* deletion in *B. bassiana* causes increased cell size and length (Cai et al. 2018). The $\Delta hos3$, $\Delta hda1$, $\Delta hst2$, and $\Delta sir2$ mutants of *A. alternata* display wild-type levels of vegetative growth and conidiation (Ma et al. 2021). These findings indicate that fungal HDACs, even close homologs, function differentially in mycelial growth and conidial development.

Besides hypersensitivity to the classical HDAC inhibitor TSA, the $\Delta Uvhos2$ strain was more sensitive to the osmotic, cell membrane, and antioxidative stresses than the wild-type and complemented strains. Similarly, the

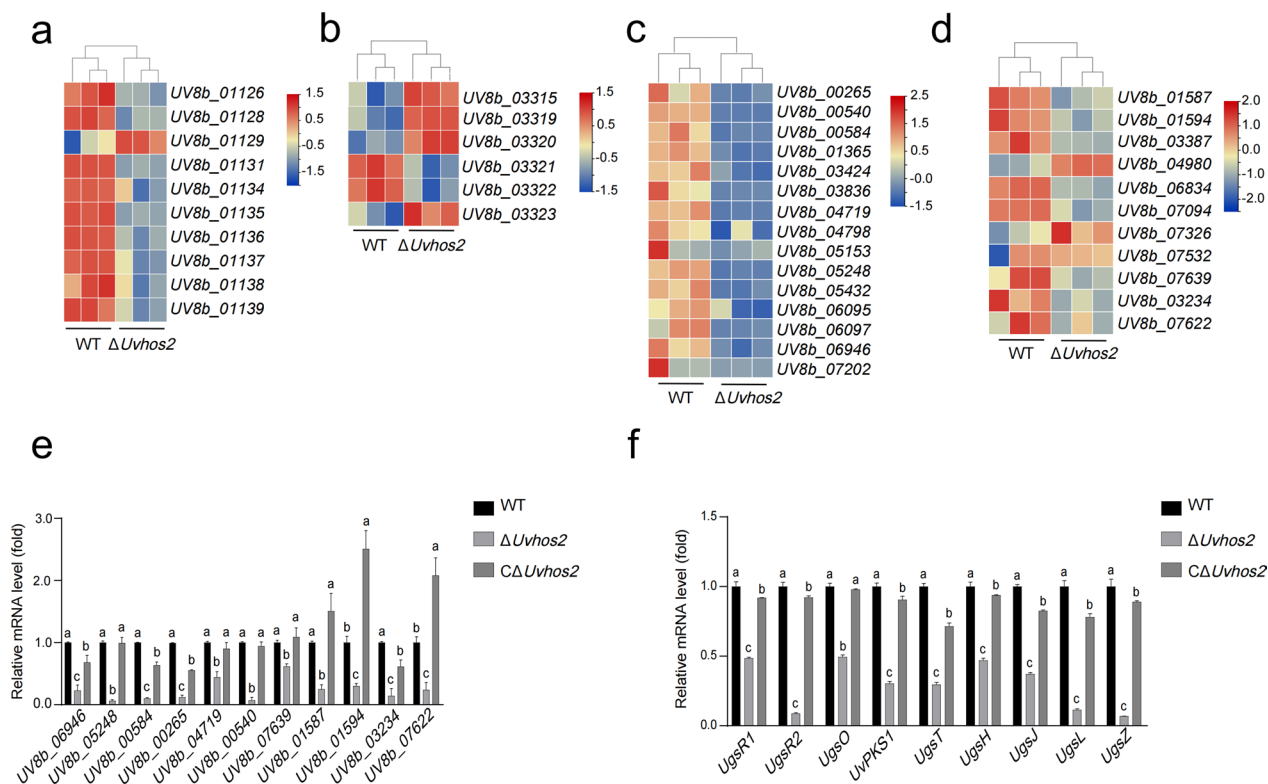


Fig. 6 UvHOS2 regulates secondary metabolism and ustilaginoidin biosynthesis in *U. virens*. Heatmaps to show the expression levels of the genes involved in the biosynthesis of ustilaginoidins **a** and sorbicillinoids **b**, and the genes encoding cytochrome P450 **c** and non-ribosomal peptide synthetases **d** associated with secondary metabolism in the wild-type and $\Delta Uvhos2$ mutant strains. Transcriptome analyses were performed with three replicates. The color column indicates the levels of gene expression that were scaled using the "Normalized" method, with red representing higher expression levels and blue indicating lower expression levels. **e, f** RT-qPCR assays to validate the expression levels of some cytochrome P450 genes, PKs genes and redox-related genes, and ustilaginoidin biosynthesis-related genes in the wild-type, $\Delta Uvhos2$, and complemented strains. The significance of differences was analyzed using one-way ANOVA with Duncan's multiple comparisons. Different lowercase letters indicate statistically significant differences ($P < 0.05$)

Colletotrichum gloeosporioides *Hos2* knockout mutants are less tolerant to oxidative and salt osmotic stresses (Liu et al. 2022). The $\Delta hos2$ mutant in *B. bassiana* exhibited a reduced tolerance to hydrogen peroxide (Cai et al. 2018). However, the deletion of the *Hos2* homologue gene *Hdf1* causes *F. graminearum* to be more tolerant to hydrogen peroxide (Li et al. 2011). These results indicate that fungal HOS2 homologs respond to environmental stresses using various mechanisms.

The phenotypic alterations after *UvHos2* deletion can be partially explained by transcriptome data. A set of genes associated with pathogenesis and conidiation are transcriptionally inhibited in the *UvHos2*-deletion mutant (Additional file 2: Table S2). Reduced virulence is also attributable to decreased conidiospore production and delayed conidial germination (Fig. 1e, f). Moreover, BLAST searches and homologous comparison revealed that some genes involved in conidial development (*UV8b_06435*, *UV8b_04229*, *UV8b_04359*, *UV8b_04568*, and *UV8b_02287*), cell wall integrity (*UV8b_03905*,

UV8b_00692), and mycelial growth (*UV8b_05833*) were down-regulated (Additional file 2: Table S2). The genes related to the biosynthesis of secondary metabolites, including ustilaginoidin biosynthesis genes, cytochrome P450 genes, and non-ribosomal peptide synthetase genes, were also significantly down-regulated (Li et al. 2019a; Liu et al. 2022; Qu et al. 2022). These data indicate that *UvHos2* plays a crucial role in secondary metabolism in *U. virens*. In addition, down-regulation of the genes related to transporters, MAPK pathways, and protein kinases disrupts normal biological processes and signaling transduction network, thus leading to the decrease of ustilaginoidin biosynthesis and the delay in growth and development in *U. virens*. Furthermore, the decreased expression of cytochrome P450 and non-ribosomal peptide synthetase genes suggests that *UvHos2* might be involved in fungal adaptation to various environmental conditions, because the two groups of enzymes are responsible for the detoxification of xenobiotics and the production of bioactive peptides, respectively (Moktali

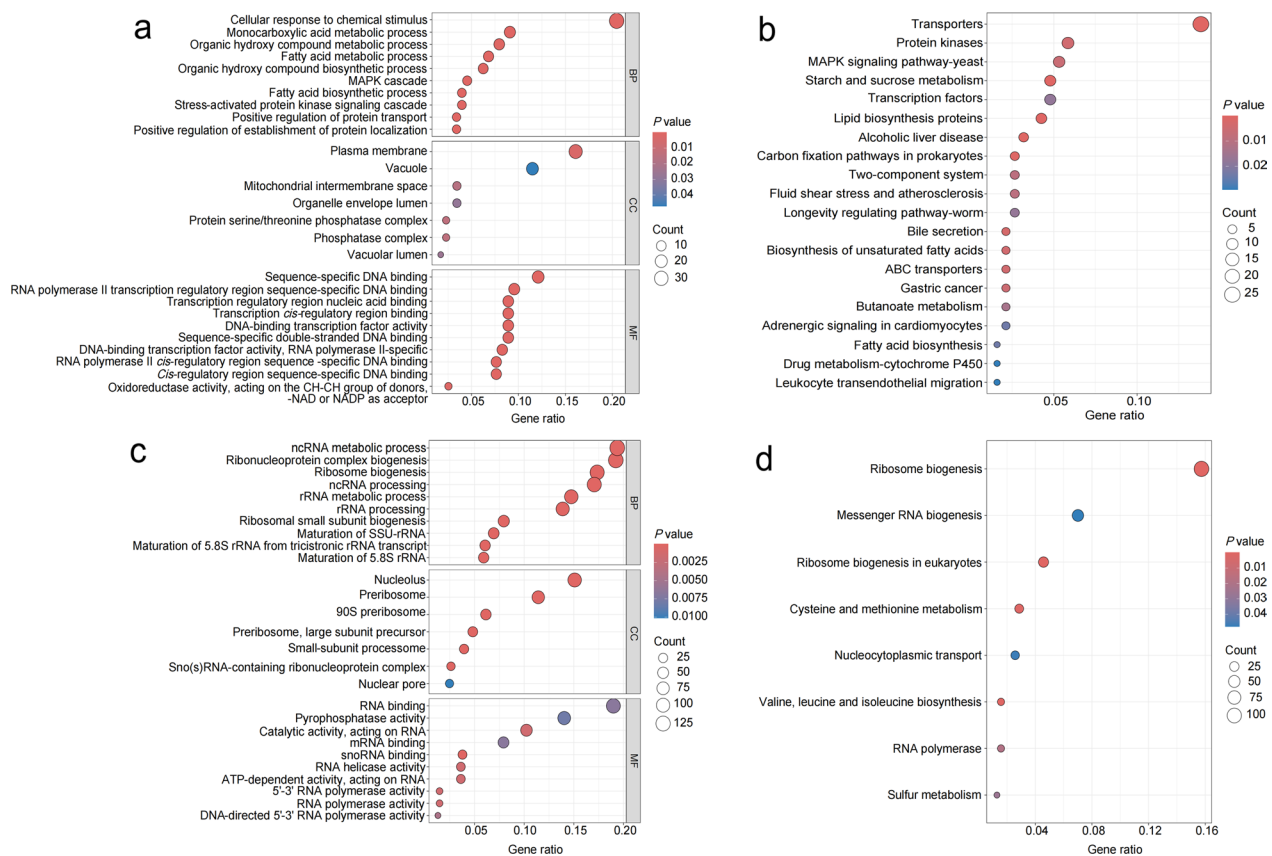


Fig. 7 GO and KEGG pathway enrichment analyses of differentially expressed genes. **a** The GO terms enriched in down-regulated genes as revealed by GO enrichment analysis. **b** The KEGG pathways enriched in down-regulated genes as revealed by KEGG enrichment analysis. **c** The GO terms enriched in up-regulated genes as revealed by GO enrichment analysis. **d** The KEGG pathways enriched in up-regulated genes as revealed by KEGG enrichment analysis. *P* values were indicated by a color bar

et al. 2012). It is interesting to investigate whether the genes involved in the synthesis of mycotoxins are essential for *U. virens* virulence. Such investigations might provide valuable insights into developing novel strategies for controlling rice false smut disease and mycotoxin contamination.

Notably, the up-regulated genes caused by *UvHos2* knockout are enriched in ribosome biogenesis, rRNA processing, and RNA binding in *U. virens*, suggesting that histone acetylation is implicated in the maturation and processing of rRNA, and ribosome assembly. Ribosomal RNAs prevent chromosome clustering (Ma et al. 2022a, b), which likely affects the synthesis of secondary metabolites, growth, and development in fungi. The 3D genome structure might facilitate elucidating molecular mechanisms of excessive rRNA in regulating the pathogenicity and secondary metabolism of *U. virens*.

UvHOS2 positively regulates ustilaginoidin production and elevates the expression of the genes involved in mycotoxin production, particularly ustilaginoidin biosynthesis. Interestingly, the gene co-expression network

analysis revealed that multiple transcription factor genes (*UV8b_03854*, *UV8b_02623*, *UV8b_03158*, *UV8b_00617*, *UV8b_00546*, and *UV8b_00825*) were linked to ustilaginoidin biosynthesis genes and were also down-regulated after the deletion of *UvHos2*, suggesting that these transcription factors regulate ustilaginoidin biosynthesis.

In fungi, histone deacetylases alter the acetylation levels at different Lys residues. The absence of *Hos2* in yeast causes an elevated H4K16 acetylation level required for high expression of growth-related genes (Wirén et al. 2005), whereas hyperacetylation occurs at the H3K18 site when *Hos2* is deleted in *M. oryzae* (Ding et al. 2010). Interestingly, we showed that the *UvHos2* mutant had significantly higher acetylation levels at H3K9, H3K14, H3K27, and H3K56 than the wild-type and complemented strains (Fig. 4). Collectively, *HOS2* homologs in diverse fungi are responsible for the deacetylation of different Lys sites in histones. Notably, *HOS2* in *M. oryzae* forms a histone deacetylase complex with Sin3, Sap18, and Sap30, which is indispensable for the maintenance of H3K27me3 occupancy and the repression of gene

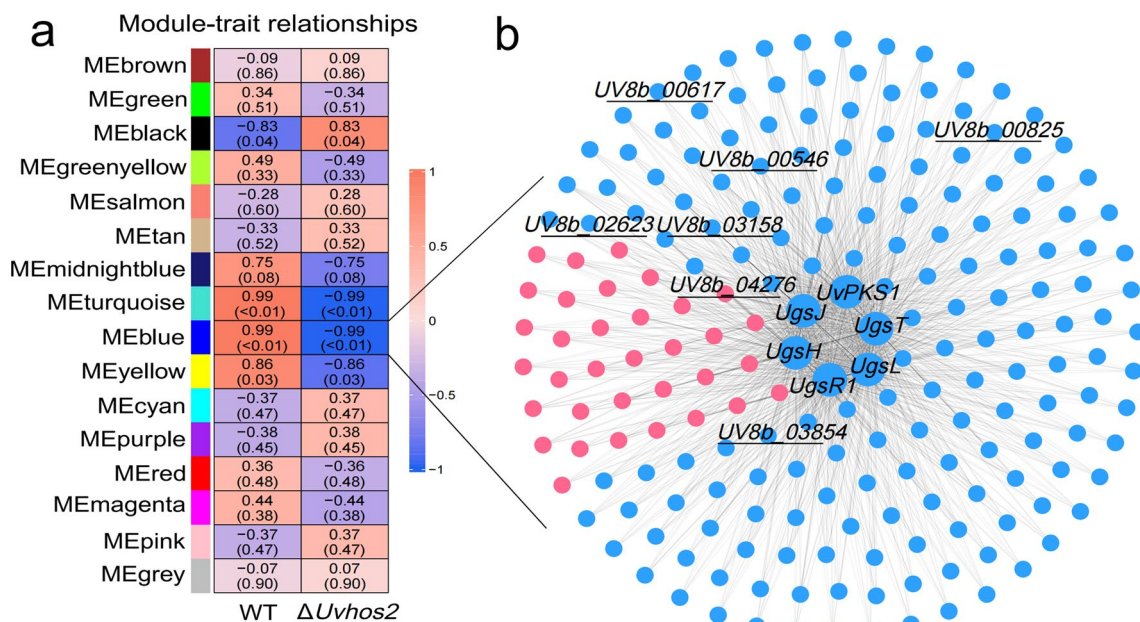


Fig. 8 WGCNA analysis reveals the co-expression gene module associated with ustilaginoidin biosynthesis. **a** The correlation analysis between module eigengenes (MEs) and traits. Each module is composed of a group of genes with a similar gene expression pattern. The heatmap showed the module-trait relationship, in which the color intensity represents the strength of positive or negative correlation. A deeper red color indicates a stronger positive correlation, while a deeper blue color indicates a stronger negative correlation. **b** The gene co-expression network in the MEblue gene module. The nodes in the network represent individual genes, while edges denote connections between genes, reflecting their similarity in expression patterns. The colors of nodes correspond to gene expression status: pink and blue represent up-regulated and down-regulated genes, respectively. The underlined genes on the nodes are annotated to encode putative transcription factors. *UvPKS1*: Polyketide synthase, *UgsJ*: Methyltransferase, *UgsH*: Hypothetical protein, *UgsR1*: Transcription initiation factor, *UgsL*: Laccase, *UgsT*: MFS multidrug transporter

expression (Lin et al. 2022). Therefore, it would be interesting to investigate whether HOS2 is associated with other transcriptional repressors to regulate secondary metabolism and gene transcription in *U. virens*.

Distinct types of HDACs differentially regulate secondary metabolism in fungi (Miyamoto et al. 2012; Ma et al. 2022a, b). The aflatoxin B1 synthesis genes are down-regulated when the class I HDAC gene *HosA/Hos2* is knocked out in *A. flavus*. ChIP-Seq analysis reveals that HOS2 directly binds to the aflatoxin synthesis genes *aflD*, *aflM*, and *aflP* to regulate aflatoxin biosynthesis (Lan et al. 2019). In contrast, multiple class II and III HDACs have been reported to negatively regulate secondary metabolism and mycotoxin synthesis. The knockout of *HdaA* significantly increases the production of penicillin and norsolorinic acid in *A. nidulans* (Shwab et al. 2007). Besides, the $\Delta sirE$ mutant exhibits an increased aflatoxin production in *A. flavus* (Wen et al. 2022), and *UvHST2* negatively regulates ustilaginoidin biosynthesis in *U. virens* (Liu et al. 2023). Interestingly, histone deacetylases are also involved in post-translational modifications, such as the removal of β -hydroxybutyrylation by *UvSirt2* and *UvSirt5* in *U. virens* (Chen et al. 2023).

The deletion of *UvHos2* leads to a significant increase in the level of H3K9 acetylation. This, in turn, inhibits the expression of *Ugs* genes but activates other important genes, as revealed by ChIP-qPCR assays (Fig. 5). Notably, H3K9ac enrichment occurs at active secondary metabolite gene clusters associated with gibberellin or fusarin C biosynthesis in *F. fujikuroi* (Niehaus et al. 2013; Studt et al. 2013), while in *A. nidulans*, H3K9ac plays a role in activating biosynthetic gene clusters for secondary metabolites, including sterigmatocystin, terrequinone, and penicillin (Nützmann et al. 2013). However, hyperacetylation of H3K9 caused by *UvHos2* deletion results in transcriptional inhibition of ustilaginoidin biosynthesis genes and a decrease in ustilaginoidin production in *U. virens*. Therefore, it is of great interest to elucidate different regulatory mechanisms involving H3K9 acetylation in distinct fungi through some novel strategies, such as Hi-C technology.

Conclusions

In this study, we have identified and characterized the class I histone deacetylase *UvHOS2* that is required for vegetative growth, conidiation, ustilaginoidin synthesis,

and pathogenicity in *U. virens*. UvHOS2 is involved in the deacetylation of histones at H3K9, H3K14, H3K27, and H3K56 in *U. virens*. Transcriptome analysis reveals the regulatory network involved in pathogenicity and secondary metabolism in *U. virens*. These findings not only provide new clues for elucidation of the molecular mechanism of epigenetic modification in regulating pathogenicity and mycotoxin biosynthesis but also lay the groundwork for the management of mycotoxin contamination.

Methods

Strains and culture conditions

The *U. virens* isolate P1 was used as the wild type for constructing gene deletion mutants. *U. virens* was cultured on potato sucrose agar (PSA, decoction of 200 g potato, 20 g sucrose, 20 g agar in 1 L ddH₂O) plates or in potato sucrose broth (PSB) at 28°C.

Construction of gene knockout and complemented strains

The gene-deletion mutants were generated through the CRISPR/Cas9 system and homologous recombination (Liang et al. 2018). Briefly, the primers S1/S2 and S5/S6 were used to amplify the upstream and downstream fragments (~1 kb) of *UvHos2*. The resultant PCR fragments of *UvHos2* were fused into 5'- and 3'-ends of the hygromycin resistance gene by fusion PCR, respectively. The sgRNA primers were designed with the sgRNA-design online tool (<https://portals.broadinstitute.org/gpp/public/analysis-tools/sgRNA-design>) and ligated into pmCas9-tRP-gRNA. The constructed plasmid and fusion PCR products were co-transformed into the protoplasts isolated from newly germinated *U. virens* hyphae via PEG-mediated transformation. The transformants were screened by PCR, and the candidate knockout mutants were confirmed by Southern blot analyses. To generate complemented strains, the *UvHos2* coding sequence was amplified and subcloned into the vector pY2P102-*Uv_08266pro:3FLAG* with a strong promoter and neomycin resistance gene (Li et al. 2019a, b). The constructed vector was introduced into the protoplasts of the knockout mutant by PEG-mediated transformation. Expression of UvHOS2-FLAG in the complemented strains was detected by western blot analysis.

Southern blot analysis

Southern blot analysis was performed as described previously (Slaton et al. 2004). Briefly, genomic DNA was extracted by the cetyltrimethyl ammonium bromide (CTAB) method. After digestion by the restriction enzyme *Sac* I, genomic DNA was separated on agarose gels and was then blotted onto the nylon membrane. The probe was amplified and labelled using a DIG High Prime

DNA Labeling and Detection Starter Kit I (Roche). The membrane was hybridized with the probe and was then visualized with NBT/BCIP chromogenic reagent.

Western blot analysis

The mycelia grown on PSA plates were collected and were then flash-frozen by liquid nitrogen. The samples were ground into powder and were added into 1×SDS loading buffer. After boiling for 10 min, the sample was centrifuged at 11,600 g for 5 min. The proteins in the supernatant were electrophoresed on 10% polyacrylamide gels and were then blotted onto PVDF membranes. The membranes were probed with an anti-FLAG antibody (Sigma). The signals were captured by a Tanon 4600SF Chemiluminescence Imaging System after the membranes were incubated with the mixture of eECL-A and eECL-B solutions (CWBI) for 3–5 min.

Conidiation and conidial germination

The wild-type, mutant, and complemented strains were cultured in PSB medium at 28°C with shaking at 150 rpm for 7 days. The conidiospores were collected by filtration through a funnel with three layers of sterilized filter paper, followed by rinsing with 25 mL of PSB medium. The conidiospores in the filtrate were counted using a hemocytometer.

The conidiospores in the filtrate were collected by centrifugation at 1200 g for 10 min. The collected conidia were resuspended in PSB medium and then adjusted to a concentration of 10⁶ spores/mL. Conidiospore suspension (100 μL) was evenly coated on PSA plates. After the plates were incubated in a 28°C incubator for 3 h, 6 h, 9 h, and 12 h, conidial germination was observed and counted under a Zeiss microscope.

Measurement of interseptal spacing

The collected conidiospores were cultured in PSB medium at 28°C with shaking at 150 rpm for germination. After 2 d culturing, the newly germinated hyphae were stained with Calcofluor White (Sigma, #18909). The interseptal lengths were measured for 100 hyphal cells of each strain with confocal microscopy. The assay was independently repeated three times.

Inoculation assay

Inoculation assay was performed as described previously (Qu et al. 2022). Briefly, *U. virens* conidial suspension, together with fragmented mycelia, was diluted to 2×10⁶ conidia/mL and was then injection-inoculated into rice panicles of the variety Changbai15 at about 7 days before heading. At least 10 rice panicles were inoculated for

each strain, and false smut balls formed on the inoculated panicles were counted at ~4 weeks after inoculation.

Tolerance to environmental stresses

To determine the sensitivity of *U. virens* mutant strains to various stress factors, *U. virens* strains were cultured on YT (0.1% yeast extract, 0.1% tryptone, and 1% glucose) medium plates supplemented with 0.5 M NaCl, 0.07% H₂O₂, 0.03% SDS, 70 µg/mL Congo Red or 1 µM TSA. After 14 d culturing at 28°C, sensitivity to various environmental stresses was evaluated by measuring colony diameter. The growth inhibition rate was calculated according to colony diameters with three technical replicates.

Detection of histone acetylation

Total proteins were extracted from the mycelia of the wild-type, mutant, and complemented strains using phosphate buffer saline (PBS) buffer. The proteins were quantified using a BCA Protein Assay Kit (Sangon Biotech, Shanghai, China). The histone acetylation levels at different Lys sites were detected by western blot analysis using different site-specific anti-acetylation antibodies, including anti-acetyl-histone H3K9, H3K14, H3K18, H3K27, H3K56, H4K5, H4K8 antibodies. H3, H4, and Actin proteins were also detected as internal controls using anti-H3, anti-H4, and anti-β-Actin antibodies (Abclonal, Wuhan, China), respectively.

Quantification of ustilaginoidins

The hyphae of the wild-type, mutant, and complemented strains were collected after culturing on PSA plates for 4 weeks at 28°C. The collected hyphae were immersed in ethyl acetate overnight, shaking at 150 rpm at 28°C. The ethyl acetate solution was then dried by rotary evaporation at 40°C, and the dried extracts were dissolved in 100% acetonitrile. After being filtered with a 0.22 µm membrane filter, ustilaginoidins were detected by high-performance liquid chromatography (LC-20A, Shimadzu, Japan). The sample (10 µL) was loaded on the Eclipse XDB-C18 column (4.6 µm × 250 mm, 5 µm) at 30°C with a flow rate of 1 mL/min under a gradient program as follows: 0–2 min, 55% acetonitrile; 2–18 min, 55–70% acetonitrile; 18–20 min, 70–100% acetonitrile; 20–28 min, 100% acetonitrile. The eluants were detected at a wavelength of 290 nm.

Transcriptome analysis

U. virens mycelia were collected for RNA isolation after 14-d culturing. RNA quality was tested by an ultraviolet-spectrophotometer. The mRNA was enriched

by magnetic beads with oligo (dT) and was then fragmented by ultrasonic. The first strand of cDNA was synthesized via the M-MLV reverse transcriptase system (TaKaRa) using fragmented mRNA as a template and random oligonucleotides as primers. RNA strand was subsequently digested with RNaseH, and the second strand of cDNA was synthesized through DNA polymerase I (CW BIO). The purified double-stranded cDNA was subjected to end repair and the addition of A-tail and the sequencing adapter. The cDNA fragments (about 200 bp) were purified by AMPure XP beads, and then PCR-amplified. The PCR products were purified by AMPure XP beads again, and finally, the library was successfully constructed for subsequent transcriptome sequencing.

RNA-seq was performed with a second-generation high-throughput sequencing Illumina platform, thus producing 150-bp paired-end raw reads. The STAR software (Dobin et al. 2013), an Ultrafast universal RNA-seq aligner, was used to map the reads to the reference genome (ASM68747v2: UV-8b) (Zhang et al. 2021), after the elimination of adapter sequences and the filtering of low-quality raw reads. Fragments Per Kilobase of exon model per Million mapped fragments (FPKM) was used to normalize the gene expression levels of the transcriptome. Genes showing an adjusted *P*-value < 0.05 and |Fold Change| > 1.5 were considered as differentially expressed genes (DEGs). The R package “pheatmap” (v1.0.12) (<https://CRAN.R-project.org/package=pheatmap>) was employed to create a heatmap showing the expression levels of P450, PKS, and non-ribosomal peptide biosynthetic-related genes in the wild-type and mutant strains.

The R package “ClusterProfiler” (Yu et al. 2012) was used to perform GO term and KEGG pathway enrichment analyses. The corrected *P*-value < 0.05 was used as a threshold for the significantly enriched GO terms and KEGG pathways. The bar plots of significant GO functional description and KEGG pathways were visualized by the “ClusterProfiler” packages. To perform the linkage among DEGs in enriched GO terms or KEGG pathways, the “cnetplot” function was used to construct the category netplot by ClusterProfiler.

RT-qPCR assay

RT-qPCR assay was performed after mRNAs were reversely transcribed into cDNAs by the PrimeScript™ RT reagent kit (TAKARA, China). The gene expression levels were detected using a LightCycler®96 real-time PCR instrument (Roche, Switzerland). The α-tubulin gene was used as an internal reference gene, and the

relative gene expression levels were calculated using the $2^{-\Delta\Delta CT}$ method (Schmittgen et al. 2000).

Weighted gene co-expression network analysis

WGCNA was implemented to identify gene modules and key regulators associated with *UvHos2* deletion using “WGCNA” package (Langfelder and Horvath 2008) in R software based on RNA-seq data. After hierarchical clustering according to the gene expression levels, the gene co-expression modules with a minimum module size of 30 genes and a merging threshold of 0.25 were identified through the dynamic tree cut method. Module eigengenes (MEs) were calculated as the first principal component for each module, which represents the overall expression pattern within the module, to infer the relationship between the identified gene modules and the *Hos2* knockout trait. Pearson correlation coefficients were then computed between MEs and traits to identify *Hos2* knockout-relevant modules. The co-expressed network was visualized by the Gephi v0.9.2 (<https://github.com/gephi/gephi/releases>) for the module significantly correlated with the knockout of *Hos2*. The egnog-mapper online program (<http://eggnog-mapper.embl.de/>) was employed to gain insights into the biological functions of the identified module.

ChIP-qPCR assay

DNA was extracted following the instructions of the ChIP Kit (IEMed-K308, China). Briefly, 7-day-old cultures of the wild-type and $\Delta Uvhos2$ strains were collected and ground into powder using liquid nitrogen. The samples were crosslinked with 1% formaldehyde in $1 \times$ PBS buffer for 10 min, and then 150 mM glycine was added to stop crosslinking. After centrifugation at 102 *g* for 5 min, the pellet was thoroughly re-suspended with 1.6 mL of IP lysis buffer with 15 μ L protease inhibitors. The cells were subject to sonication on an ice bath for 30–50 min. Subsequently, the binding enhancer buffer (400 μ L) was added. After centrifugation at 12,000 *g* at 4°C for 10 min, the supernatants were mixed with 20 μ L of clean beads and were then incubated at room temperature for 20 min. Protein A/G beads were pre-incubated with anti-acetyl-H3K9 antibody (Abcam, A7255) or IgG in AB binding buffer on a rotary shaker for 30 min. The supernatants (900 μ L) were incubated with antibody- or IgG-pretreated Protein A/G beads on a rotary shaker at room temperature for 1 h. The beads were rinsed with 500 μ L of ChIP washing buffer three times. Finally, immunoprecipitated DNA was eluted with 30 μ L of elution buffer. ChIP-qPCR was performed using immunoprecipitated DNA as a template. The qRT-PCR primers were listed in Additional file 2: Table S3.

Abbreviations

CTAB	Cetyltrimethyl ammonium bromide
DEGs	Differentially expressed genes
FPKM	Fragments per kilobase of exon model per million mapped fragments
GO	Gene ontology
HAT	Histone acetyltransferases
HDAC	Histone deacetylases
HPLC	High performance liquid chromatography
KEGG	Kyoto encyclopedia of genes and genomes
PBS	Phosphate buffer saline
PKS	Polyketide synthase
PSA	Potato sucrose agar
RNA-Seq	RNA sequencing
TSA	Trichostatin A
WGCNA	Weighted gene co-expression network analysis
YT	Yeast extract-tryptone

Supplementary Information

The online version contains supplementary material available at <https://doi.org/10.1186/s42483-024-00230-3>.

Additional file 1: Figure S1. The phylogenetic tree and domain architectures of class I histone deacetylases in *U. virens* and other related fungal species. **a** The phylogenetic tree of the class I HDACs in *U. virens* and eight related fungal species (*A. alternata*, *A. flavus*, *B. bassiana*, *C. albicans*, *U. maydis*, *F. graminearum*, *M. oryzae*, and *S. cerevisiae*). The evolutionary tree was constructed using the maximum likelihood method. Bootstrap values based on 1000 replicates were shown at nodes. **b** The conserved domain architectures of class I HDACs in the related fungal species. The rectangles represent the conserved domains with the indicated length of domains. Distinct types of domains are indicated by different colors. The scale bar indicates the number of substitutions per amino acid residue. **Figure S2.** Southern blot and western blot analyses to confirm the knockout and complemented strains of the deacetylase gene *UvHos2* in *U. virens*. **a** A schematic diagram to show the probe design strategy to confirm the *UvHos2* deletion mutant. **b** Southern blot analysis to confirm the $\Delta UvHos2$ knockout mutants. WT, the wild-type strain. **c** The expression levels of *UvHos2*-FLAG in different $C\Delta UvHos2$ complemented strains were detected by western blot analysis with an anti-FLAG antibody. The $\Delta UvHos2$ knockout mutant was used as a negative control. **Figure S3.** Volcano plot showing differentially expressed genes between the wild-type and $\Delta UvHos2$ strains ($|\text{Fold Change}| > 1.5$ and $P\text{-value} < 0.05$). Red and blue dots represent up-regulated and down-regulated genes, respectively, while gray dots indicate the genes with no change in expression.

Additional file 2: Table S1. The annotation of the differentially expressed genes related to *Ugs* genes in MEblue module. **Table S2.** The homologous proteins in *U. virens* identified based on sequence similarity to the proteins known for pathogenicity, cell wall integrity, conidial generation, or mycelial growth in other fungi. **Table S3.** The primers used in this study.

Acknowledgements

We thank Jinrong Xu at Purdue University for the vector pCAS9-tRp-gRNA, Yongfeng Liu at the Institute of Plant Protection, Jiangsu Academy of Agricultural Sciences for the *U. virens* strain P1.

Author contributions

ZYL and WXS designed the experiments. ZYL, PYW, QHY, BW, DYL, CY, LL, and GHD performed the experiments and collected data. ZYL and GHD performed data analyses. ZYL, GHD, and WXS wrote and revised the manuscript. All authors read and approved the final manuscript.

Funding

The work is supported by the National Natural Science Foundation of China (NSFC) Grants (32293241 and U19A2027 to WS and 32302336 to GD), and the earmarked funds for China Agricultural Research System (CARS01) to WS.

Availability of data and materials

The datasets used and/or analyzed in this study are available from the corresponding authors on request.

Declarations**Ethical approval and consent to participate**

Not applicable.

Consent for publication

Not applicable.

Competing interests

The authors declare that they have no competing interests.

Received: 18 August 2023 Accepted: 23 January 2024

Published online: 07 March 2024

References

- Baidyaroy D, Brosch G, Ahn J-h, Graessle S, Wegener S, Tonukari NJ, et al. A gene related to yeast HOS2 histone deacetylase affects extracellular depolymerase expression and virulence in a plant pathogenic fungus. *The Plant Cell*. 2001;13:1609–24. <https://doi.org/10.1105/tpc.010168>.
- Bauer I, Misslinger M, Shadkhan Y, Dietl A-M, Petzer V, Orasch T, et al. The lysine deacetylase RpdA is essential for virulence in *Aspergillus fumigatus*. *Front Microbiol*. 2019;10:2773. <https://doi.org/10.3389/fmicb.2019.02773>.
- Cai Q, Tong S-M, Shao W, Ying SH, Feng MG. Pleiotropic effects of the histone deacetylase Hos2 linked to H4–K16 deacetylation, H3–K56 acetylation, and H2A–S129 phosphorylation in *Beauveria bassiana*. *Cell Microbiol*. 2018;20: e12839. <https://doi.org/10.1111/cmi.12839>.
- Chen X, Duan Y, Ren Z, Niu T, Xu Q, Wang Z, et al. Post-translational modification β -hydroxybutyrylation regulates *Ustilagoidea virens* virulence. *Mol Cell Proteom*. 2023. <https://doi.org/10.1016/j.mcpro.2023.100616>.
- Ding S-L, Liu WD, Iliuk AT, Ribot C, Vallet J, Tao A, et al. The Tig1 histone deacetylase complex regulates infectious growth in the rice blast fungus *Magnaporthe oryzae*. *Plant Cell*. 2010;22:2495–508. <https://doi.org/10.1105/tpc.110.074302>.
- Dobin A, Davis CA, Schlesinger F, Drenkow J, Zaleski C, Jha S, et al. STAR: ultra-fast universal RNA-seq aligner. *Bioinformatics*. 2013;29:15–21. <https://doi.org/10.1093/bioinformatics/bts635>.
- Ekwall K. Genome-wide analysis of HDAC function. *Trends Genet*. 2005;21:608–15. <https://doi.org/10.1016/j.tig.2005.08.009>.
- Fu XX, Xie RS, Wang J, Chen X, Wang X, Sun W, et al. Development of colloidal gold-based lateral flow immunoassay for rapid qualitative and semi-quantitative analysis of ustiloxins A and B in rice samples. *Toxins*. 2017;9:79. <https://doi.org/10.3390/toxins9030079>.
- Grunstein M. Histone acetylation in chromatin structure and transcription. *Nature*. 1997;389:349–52. <https://doi.org/10.1038/38664>.
- Guzman-Chavez F, Salo O, Samol M, Ries M, Kuipers J, Bovenberg RA, et al. Deregulation of secondary metabolism in a histone deacetylase mutant of *Penicillium chrysogenum*. *Microbiol Open*. 2018;7:e00598. <https://doi.org/10.1002/mbo3.598>.
- Hnisz D, Bardet AF, Nobile CJ, Petryshyn A, Glaser W, Schöck U, et al. A histone deacetylase adjusts transcription kinetics at coding sequences during *Candida albicans* morphogenesis. *PLoS Genet*. 2012;8:e1003118. <https://doi.org/10.1371/journal.pgen.1003118>.
- Kawauchi M, Nishiura M, Iwashita K. Fungus-specific sirtuin HstD coordinates secondary metabolism and development through control of LaeA. *Eukaryot Cell*. 2013;12:1087–96. <https://doi.org/10.1128/ec.00003-13>.
- Lai DW, Meng JJ, Zhang XP, Xu D, Dai J, Zhou L. Ustilobisorbicillinol A, a cytotoxic sorbyl-containing aromatic polyketide from *Ustilagoidea virens*. *Org Lett*. 2019;21:1311–4. <https://doi.org/10.1021/acs.orglett.8b04101>.
- Lan HH, Wu LH, Sun RL, Keller NP, Yang K, Ye L, et al. The HosA histone deacetylase regulates aflatoxin biosynthesis through direct regulation of aflatoxin cluster genes. *Mol Plant Microbe Interact*. 2019;32:1210–28. <https://doi.org/10.1094/MPMI-01-19-0033-R>.
- Langfelder P, Horvath S. WGCNA: an R package for weighted correlation network analysis. *BMC Bioinform*. 2008;9:1–13. <https://doi.org/10.1186/1471-2105-9-559>.
- Lee SH, Farh ME-A, Lee J, Oh YT, Cho E, Park J, et al. A histone deacetylase, *Magnaporthe oryzae* RPD3, regulates reproduction and pathogenic development in the rice blast fungus. *mBio*. 2021;12:e02600-21. <https://doi.org/10.1128/mBio.02600-21>.
- Li YM, Wang CF, Liu WD, Wang G, Kang Z, Kistler HC, et al. The *HDF1* histone deacetylase gene is important for conidiation, sexual reproduction, and pathogenesis in *Fusarium graminearum*. *Mol Plant Microbe Interact*. 2011;24:487–96. <https://doi.org/10.1094/MPMI-10-10-0233>.
- Li X, Pan L, Wang B, Pan L. The histone deacetylases HosA and HdaA affect the phenotype and transcriptomic and metabolic profiles of *Aspergillus niger*. *Toxins*. 2019a;11:520. <https://doi.org/10.3390/toxins11090520>.
- Li YJ, Wang M, Liu ZH, Zhang K, Cui F, Sun W. Towards understanding the biosynthetic pathway for ustilaginoidin mycotoxins in *Ustilagoidea virens*. *Environ Microbiol*. 2019b;21:2629–43. <https://doi.org/10.1111/1462-2920.14572>.
- Liang Y, Han Y, Wang C, Jiang C, Xu J-R. Targeted deletion of the USTA and UvSLT2 genes efficiently in *Ustilagoidea virens* with the CRISPR-Cas9 system. *Front Plant Sci*. 2018;9:699. <https://doi.org/10.3389/fpls.2018.00699>.
- Lin CX, Cao X, Qu ZW, Zhang SI, Naqvi NI, Deng YZ. The histone deacetylases MoRpd3 and MoHst4 regulate growth, conidiation, and pathogenicity in the rice blast fungus *Magnaporthe oryzae*. *MSphere*. 2021;6:e00118-21. <https://doi.org/10.1128/msphere.00118-21>.
- Lin C, Wu Z, Shi H, Yu J, Xu M, Lin F, et al. The additional PRC2 subunit and Sin3 histone deacetylase complex are required for the normal distribution of H3K27me3 occupancy and transcriptional silencing in *Magnaporthe oryzae*. *New Phytol*. 2022;236:576–89. <https://doi.org/10.1111/nph.18383>.
- Liu SK, Wang QN, Liu N, Luo H, He C, An B. The histone deacetylase HOS2 controls pathogenicity through regulation of melanin biosynthesis and appressorium formation in *Colletotrichum gloeosporioides*. *Phytopathol Res*. 2022;4:1–13. <https://doi.org/10.1186/s42483-022-00126-0>.
- Liu L, Wang B, Duan GH, Wang J, Pan ZQ, Ou MM, et al. Histone deacetylase UvHST2 is a global regulator of secondary metabolism in *Ustilagoidea virens*. *J Agric Food Chem*. 2023. <https://doi.org/10.1021/acs.jafc.3c01782>.
- Lu Y, Su C, Liu HP. A GATA transcription factor recruits Hda1 in response to reduced Tor1 signaling to establish a hyphal chromatin state in *Candida albicans*. *PLoS Pathog*. 2012;8:e1002663. <https://doi.org/10.1371/journal.ppat.1002663>.
- Lu SQ, Sun WB, Meng JJ, Wang A, Wang X, Tian J, et al. Bioactive bis-naphthopyrones from rice false smut pathogen *Ustilagoidea virens*. *J Agric Food Chem*. 2015;63:3501–8. <https://doi.org/10.1021/acs.jafc.5b00694>.
- Ma HJ, Li L, Gai YP, Zhang X, Chen Y, Zhuo X, et al. Histone acetyltransferases and deacetylases are required for virulence, conidiation, DNA damage repair, and multiple stresses resistance of *Alternaria alternata*. *Front Microbiol*. 2021;12:783633. <https://doi.org/10.3389/fmicb.2021.783633>.
- Ma XY, Jiang YR, Ma LX, Luo S, Du H, Li X, et al. Corepressors SsnF and RcoA regulate development and aflatoxin B₁ biosynthesis in *Aspergillus flavus* NRRL 3357. *Toxins*. 2022a;14:174. <https://doi.org/10.3390/toxins14030174>.
- Ma K, Luo M, Xie G, Wang X, Li Q, Gao L, et al. Ribosomal RNA regulates chromosome clustering during mitosis. *Cell Discov*. 2022b;8:51. <https://doi.org/10.1038/s41421-022-00400-7>.
- Maeda K, Izawa M, Nakajima Y, Jin Q, Hirose T, Nakamura T, et al. Increased metabolite production by deletion of an HDA1-type histone deacetylase in the phytopathogenic fungi, *Magnaporthe oryzae* (*Pyricularia oryzae*) and *Fusarium asiaticum*. *Lett Appl Microbiol*. 2017;65:446–52. <https://doi.org/10.1111/lam.12797>.
- Meng JJ, Sun WB, Mao ZL, Xu D, Wang X, Lu S, et al. Main ustilaginoidins and their distribution in rice false smut balls. *Toxins*. 2015;7:4023–34. <https://doi.org/10.3390/toxins7104023>.
- Miyamoto M, Furuichi Y, Komiyama T. The high-osmolarity glycerol- and cell wall integrity-MAP kinase pathways of *Saccharomyces cerevisiae* are involved in adaptation to the action of killer toxin HM-1. *Yeast*. 2012;29:475–85. <https://doi.org/10.1002/yea.2927>.
- Moktali V, Park J, Fedorova-Abrams ND, Park B, Choi J, Lee Y-H, et al. Systematic and searchable classification of cytochrome P450 proteins encoded by fungal and oomycete genomes. *BMC Genom*. 2012;13:1–13. <https://doi.org/10.1186/1471-2164-13-525>.
- Niehues E-M, Kleigrew K, Wiemann P, Studt L, Sieber CM, Connolly LR, et al. Genetic manipulation of the *Fusarium fujikuroi* fusarin gene cluster yields

- insight into the complex regulation and fusarin biosynthetic pathway. *Chem Biol.* 2013;20:1055–66. <https://doi.org/10.1016/j.chembiol.2013.07.004>.
- Nützmann H-W, Fischer J, Scherlach K, Hertweck C, Brakhage AA, et al. Distinct amino acids of histone H3 control secondary metabolism in *Aspergillus nidulans*. *Appl Environ Microbiol.* 2013;79:6102–9. <https://doi.org/10.1128/AEM.01578-13>.
- Qiu JH, Meng S, Deng YZ, Huang SW, Kou YJ. *Ustilagoidea virens*: A fungus infects rice flower and threatens world rice production. *Rice Sci.* 2019;26:199–206. <https://doi.org/10.1016/j.rsci.2018.10.007>.
- Qu J, Wang Y, Cai M, Liu Y, Gu L, Zhou P, et al. The bZIP transcription factor UvbZIP6 mediates fungal growth, stress response, and false smut formation in *Ustilagoidea virens*. *Phytopathol Res.* 2022;4:1–12. <https://doi.org/10.1186/s42483-022-00137-x>.
- Schmittgen TD, Zakrajsek BA, Mills AG, Gorn V, Singer MJ, Reed MW. Quantitative reverse transcription–polymerase chain reaction to study mRNA decay: comparison of endpoint and real-time methods. *Anal Biochem.* 2000;285:194–204. <https://doi.org/10.1006/abio.2000.4753>.
- Shwab EK, Bok JW, Tribus M, Galehr J, Graessle S, Keller NP. Histone deacetylase activity regulates chemical diversity in *Aspergillus*. *Eukaryot Cell.* 2007;6:1656–64. <https://doi.org/10.1128/ec.00186-07>.
- Slaton NA, Gbur EE Jr, Cartwright RD, DeLong RE, Norman RJ, Brye KRJA. Grain yield and kernel smut of rice as affected by pre-flood and midseason nitrogen fertilization in Arkansas. *Agron J.* 2004;96:91–9. <https://doi.org/10.2134/agronj2004.9100>.
- Studt L, Schmidt F, Jahn L, Sieber C, Connolly L, Niehaus E-M, et al. Two histone deacetylases, FfHda1 and FfHda2, are important for *Fusarium fujikuroi* secondary metabolism and virulence. *Appl Environ Microbiol.* 2013;79:7719–34. <https://doi.org/10.1128/AEM.01557-13>.
- Sun WB, Wang AL, Xu D, Wang W, Meng J, Dai J, et al. New ustilaginoidins from rice false smut balls caused by *Villosiclava virens* and their phytotoxic and cytotoxic activities. *J Agric Food Chem.* 2017;65:5151–60. <https://doi.org/10.1021/acs.jafc.7b01791>.
- Sun WX, Fan J, Fang AF, Li Y, Tariqjaveed M, Li D, et al. *Ustilagoidea virens*: insights into an emerging rice pathogen. *Annu Rev Phytopathol.* 2020;58:363–85. <https://doi.org/10.1146/annurev-phyto-010820-012908>.
- Tribus M, Bauer I, Galehr J, Rieser G, Trojer P, Brosch G, et al. A novel motif in fungal class 1 histone deacetylases is essential for growth and development of *Aspergillus*. *Mol Biol Cell.* 2010;21:345–53. <https://doi.org/10.1091/mbc.09-08-0750>.
- Trojer P, Brandtner EM, Brosch G, Loidl P, Galehr J, Linzmaier R, et al. Histone deacetylases in fungi: novel members, new facts. *Nucleic Acids Res.* 2003;31:3971–81. <https://doi.org/10.1093/nar/gkg473>.
- Wang B, Liu L, Li YJ, Zou J, Li D, Zhao D, et al. Ustilaginoidin D induces hepatotoxicity and behaviour aberrations in zebrafish larvae. *Toxicology.* 2021;456:152786. <https://doi.org/10.1016/j.tox.2021.152786>.
- Wen M, Lan H, Sun R, Chen X, Zhang X, Zhu Z, et al. Histone deacetylase SirE regulates development, DNA damage response and aflatoxin production in *Aspergillus flavus*. *Environ Microbiol.* 2022;24:5596–610. <https://doi.org/10.1111/1462-2920.16198>.
- Wirén M, Silverstein RA, Sinha I, Walfridsson J, Hm Lee, Laurensen P, et al. Genome wide analysis of nucleosome density histone acetylation and HDAC function in fission yeast. *EMBO J.* 2005;24:2906–18. <https://doi.org/10.1038/sj.emboj.7600758>.
- Yu G, Wang L-G, Han Y, He Q-Y. ClusterProfiler: an R package for comparing biological themes among gene clusters. *Omic J Integr Biol.* 2012;16:284–7. <https://doi.org/10.1089/omi.2011.0118>.
- Zhang Y, Zhang K, Fang AF, Han Y, Yang J, Xue M, et al. Specific adaptation of *Ustilagoidea virens* in occupying host florets revealed by comparative and functional genomics. *Nat Commun.* 2014;5:1–12. <https://doi.org/10.1038/ncomms4849>.
- Zhang N, Yang ZZ, Zhang ZH, Liang W. BcRPD3-mediated histone deacetylation is involved in growth and pathogenicity of *Botrytis cinerea*. *Front Microbiol.* 2020;11:1832. <https://doi.org/10.3389/fmicb.2020.01832>.
- Zhang K, Zhao ZX, Zhang ZD, Li YJ, Li SJ, Yao N, et al. Insights into genomic evolution from the chromosomal and mitochondrial genomes of *Ustilagoidea virens*. *Phytopathol Res.* 2021;3:9. <https://doi.org/10.1186/s42483-021-00086-x>.